Drag Reducing and Cavitation Resistant Coatings

Executive Summary

Client, Green Building Systems (GBS), presented PNNL a coating designed by Intuitive Coatings reported to reduce drag and prevent cavitation damage on marine vessels, turbines and pumps. The composition of the coating remains proprietary but includes silicon oxides, aliphatic carbon chains, and fluorine-rich particles. The coating is spray applied to surfaces. Prior GBS testing and experiments suggest reduction of both drag and cavitation damage on industrial scale propellers, but the underlying mechanism for these effects remains unclear.[1] Yet, the application is compelling because even modest reductions in drag to marine vessels and cavitation damage to propellers and turbines present a significant economic and environmental opportunity.

PNNL considered possible mechanisms with the client, executed multiple experiments, and completed one theoretical analysis (see appendix). The remainder of this report first considers image analysis to gain insight into drag reduction mechanisms and then exposes the coating to cavitation to explore its response to an intensely cavitating environment. Although further efforts may be warranted to confirm mechanisms, this report presents a first investigation into these coatings within the scope and resources of the technology assistance program (TAP).

Image Analysis

Samples comprising GBS's proprietary coating on top of a grey colored paint on a fiberglass hull were prepared by GBS. The coating was applied by spraying in triplicate with drying for at least 24 hours before the samples were shipped to PNNL. At the Environmental and Molecular Sciences Laboratory (EMSL), these coatings were characterized using a Helios Nanolab dual-beam focused ion beam/scanning electron microscopy (FIB/SEM) microscope.[2] To facilitate imaging, a thin conductive carbon layer was deposited on two of the samples to minimize charging. Without this conductive layer, a layer of electrons accumulated on the surface of the sample, indicating that the underlying surface material is largely insulating with minimal electron transfer. Visual observation of the surface showed it to be largely smooth without large undulations or regularly spaced riblets (see Figure 1).[3] Occasional protrusions were visible on the surface. Energy dispersive X-ray spectroscopy (EDXS) far from the protrusions found a surface rich in carbon, oxygen, and silicon, while the protrusions were enriched in a fluorine-containing compound (see Table 1). A rectangular layer of 45% platinum and 55% carbon was deposited on the surface to facilitate Ga-69 etching of the surface. The etched pit was 55 microns by 60 microns in lateral dimensions and at least 20 microns deep (see Figure 2). Imaging the sidewall of the etched pit found the coating to be typically 6-8 microns (0.24-0.31 mils) thick. Below the coating, EDXS discovered small but significant concentrations of titanium, magnesium, and the absence of chlorine, characteristic of the grey paint and not the proprietary coating. The etching of the coating appeared to be more challenging than etching of the paint with evidence of "curtaining" and weak channeling, consistent with a more rigid coating than the softer underlying paint (see Figure 2). The appearance of the coating was amorphous and non-crystalline comprising a continuous matrix with two types of discrete phases. Both of the discrete phases are darker in the imaging, suggesting lower electron density, and one of the discrete phases was more resistant to etching than the other (see Figure 3 right).

[1] GBS data not independently reviewed as part of this effort.
[2] https://www.emsl.pnl.gov/emslweb/instruments/helios-fibsem, downloaded 1/20/2016.
[3] http://rsta.royalsocietypublishing.org/content/368/1929/4775, downloaded 1/20/2016.

The discrete phases were not preferentially accumulated at the surface. Significant evidence of micron-scale holes was not observed. The coating formed an integral boundary with the underlying paint without evidence of fracture or mismatch at the junction.

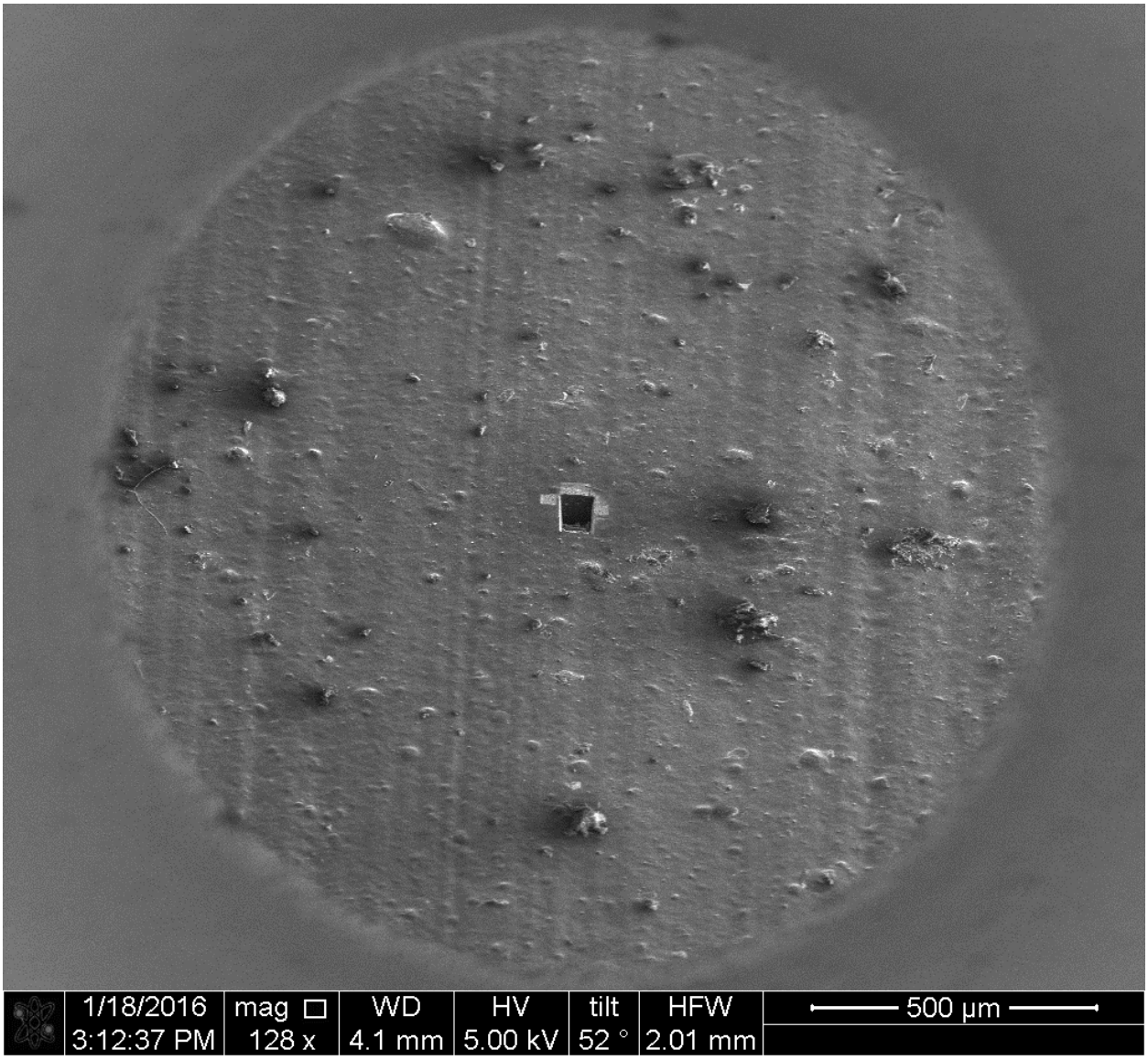

Figure 1. Electron microscopy image of the surface of the carbon coated sample. The dark square in the middle is the etched location represented in the other figures and is approximately 55 microns wide. The gradual undulations observed at this scale are much larger in period than the characteristic thickness of the coating (6-8 microns), suggesting that the undulations arise from the underlying paint surface not the sprayed on coating.

Table 1. Atomic compositions by percent

	Coating	Paint	Bright Feature in Paint	Top Surface	Bright Feature on Top Surface
C	69.16±2.88	78.89±9.60	22.46	67.76	66.29
O	16.70±2.32	9.34±2.89	44.76	26.13	14.64
F	1.87	-	-	-	15.15
Mg	-	0.68±0.27	11.67	-	-
Si	11.00±2.47	8.81±4.72	20.15	4.99	3.36
Cl	2.06±0.33	-	-	1.04	0.50
Ti	-	2.74±2.33	0.29	0.09*	0.05*
Ga**	0.62±0.15	0.46±0.09	0.68	-	-

*These titanium compositions may result from material sprayed out of the pit during etching of the paint layer.
**Ga composition here comes from the etching process and was not likely present in the original sample.

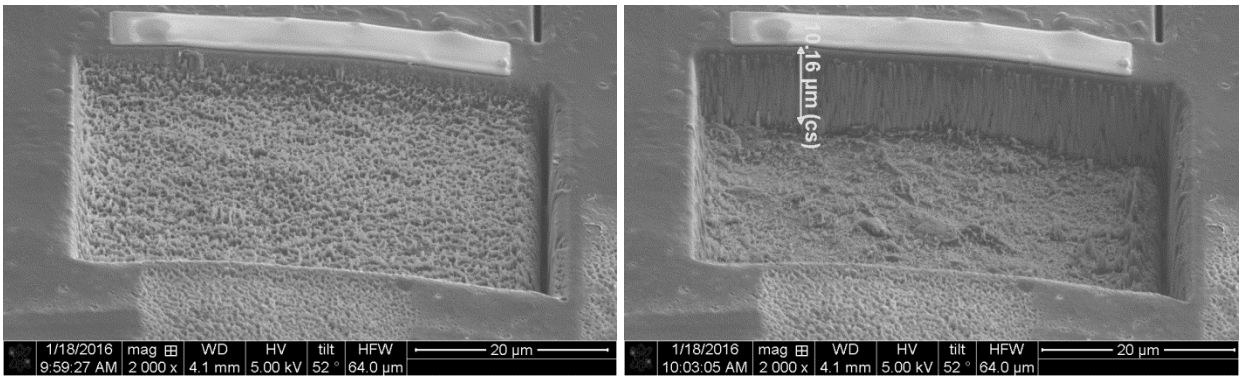

Figure 2. Top view of etching through (left) coating and (right) paint layers, leaving distinctive surface topologies. The channeling on the left is formed by Ga-69 bombardment. The rectangular bar above the pit is a made of platinum and carbon.

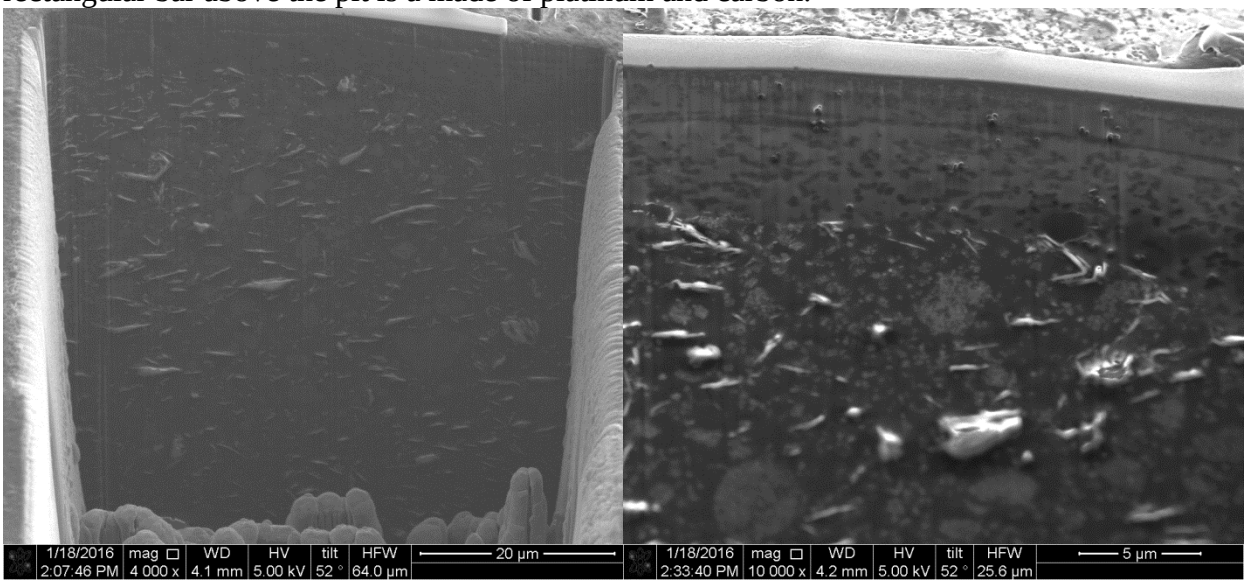

Figure 3. Cross sectional views showing both coating and paint layers at different magnifications (see scale bar). The image on the right shows a light matrix with two types of dark particles embedded. The particles seen as dark circles with bright outline are likely harder than the other dark particles.

In addition to imaging, the static wetting behavior of the coating was observed. Small droplets were placed on a coated surface. Visual observation of water droplets on this surface suggests a contact angle between 30 and 60 degrees, consistent with a wetting surface. The dynamic contact angle and the dynamic contact angle in the presence of an electric field were not evaluated in this report.

In light of these observations, this report begins the process of evaluating the underlying mechanism for effects observed by GBS. Several mechanisms may be responsible for drag reduction including:

- Super-hydrophobic surfaces with small scale roughness or hydrophobic surface chemistries may reduce drag. However, the static contact angle and client provided video suggests that the surfaces are wetting typical of hydrophilic surfaces instead of non-wetting characteristic of hydrophobic surface. Super-hydrophobic contact angles were not observed, but dynamic contact angles with and without electrical fields were also not explored.
- Trapped microbubbles may be associated with drag reduction. However, visual observation did not suggest surfaces that would trap microbubbles. In fact, visualization of wetting suggests exactly the opposite that microbubbles would be released instead of trapped to reduce surface energy.
- Reducing the roughness of exposed surfaces is well known to affect the turbulent drag across surfaces, and external flow across large vessels (e.g., 1300 ft) shortly becomes turbulent. The coating is only 6-8 microns thick in the regions analyzed. This suggests that the coating only minimally affects the surface roughness.
- Biomimetic riblets have been argued to decrease drag by up to 10%.[4] Visual observations do not suggest regularly spaced undulations or riblets required for drag reduction. In contrast, the protrusions observed are characteristic of normal randomly distributed surface roughness, which would increase drag instead of reduce it.
- Some polymer coatings, particle-rich surfaces, and surface charge may introduce a slip length that may or may not be associated with drag reduction. This mechanism cannot be conclusively included or excluded based on the work performed to date.
- Finally, electrohydrodynamic effects may be responsible for drag reduction. This option is of particular interest to the client and hence the appendix at the end of this report. Because seawater is net neutral, electrohydrodynamic effects must arise at moving surfaces. Several possible sources of surface charging or electrostatic surface potential may be considered.
    - First, surface charging may arise from conduction through the bulk of the coating up to the surface. Although weak channeling may have been observed, given the insulating nature of the coating (addition of a conductive layer was required to disperse electrons away from the surface) significant rates of electron transfer from the substrate through the paint and then through the coating would be unexpected.
    - Second, the surface potential may arise from piezoelectric effects. Quartz exhibits the piezoelectric effect whereas silica does not because the piezoelectric effect in ceramics arises from crystalline structures or regularly oriented inclusions. Neither crystalline structures nor regularly oriented inclusions were

[4] http://rsta.royalsocietypublishing.org/content/368/1929/4775, downloaded 1/20/2016.

observed. Because absence of evidence is non-conclusive, additional tests for piezo-electricity could be performed to evaluate this possibility. However, the client-performed experiment to remove the induced surface charge by cleaning with detergent should have had little effect because piezo-electricity is a bulk effect instead of a surface effect.

- Third, the surface charge may develop due to ionization of a silica rich surface. It is well known that hydroxyl groups may be present on the surface and may ionize in the presence of water. This is the most likely mechanism for the development of surface charge. The fluorine enriched protrusions may or may not have also contributed.
- Fourth, one other possibility is the development of a surface charge due to differences in electron affinities between the coating and seawater.

Further evaluation of the sources of surface charge lies outside the scope of this report and FY16 TAP effort.

Cavitation Resistance

This effort also considered potential cavitation resistance provided by the coating. Samples comprising GBS's proprietary coating, which differ in some respects from the coating above, were prepared by GBS. The coating was applied to a metallic surface before the samples were shipped to PNNL. Client-provided samples include two each of an untreated metallic sample (labeled U in Figure 4), T2 Marine (labeled W), and T2 Marine with aluminum (labeled A). Each sample was mostly visually flat though a small curvature before and after testing may be observed in Figure 4. One of each pair was secured to a chuck made out of transparent acrylic using superglue. The chuck was positioned within a beaker using rubber stoppers. Securing the samples prevents movement or displacement when the samples are exposed to sonication, ensuring that the same area is repeatedly exposed to cavitation generated bubbles. The cavitation experiment was performed using a Sonics and Materials VC-750 sonicator with a 630-0418 tapered microtip. This tip was selected because the manufacturer indicated that "Two types of microtips are available to enable processing samples in small vessels at very high intensity – a tapered microtip and a stepped microtip"[5] and very intense cavitation fields were desired to mimic longer term commercial performance in a short laboratory experiment. The exact correspondence between industrial exposure and the fields in this experiment has not been established. The cavitation exposure may have been more or less intense than a coating would have experienced in service. The tip probe was positioned at the junction of the three samples approximately 5 mm above the sample surface. The samples were exposed to sonication energy at the 40% intensity setting for over three hours at 10-60 minute intervals. The experiment was terminated when the probe showed signs of visible damage at the tip. The tapered microtip was constructed out of titanium alloy Ti-6Al-4V and the induced cavitation was sufficiently intense to damage the metallic microtip.

Careful observation of Figure 4 shows unusual discoloration of the exposed samples near the junction after 145 minutes of cavitation exposure (see panel e). Detailed observation of panel c suggests that the same features were present 40 minutes into the experiment but not after only 10 minutes. To further evaluate the surface topology, each sample surface was profiled before

[5] Ultrasonic horn probes are on page 13 of http://www.sonics.com/catalog.pdf, downloaded 9-29-2016.

and after exposure using a surface profilometer (Veeco Dektak 150).[6] This instrument works much like an old record player. A tip similar to a record player needle moves across the surface. As it moves up and down, an electronic signal is generated that converts into a precise representation of the surface topology as seen in Figure 5. This figure shows that the profiles are quite smooth before exposure. (The uncoated sample had some edging similar to a postage stamp that may affect results.) After 205 minutes of exposure, the uncoated sample shows a jagged edge under the tapered microtip (Figure 5a). Similarly, after 205 minutes of exposure, the coated sample shows a jump in the profile under the tapered microtip (Figure 5b) as circled in (dotted) purple that was not there previously. The cause of the jump remains unclear, but, in conjunction with the observed discoloration in Figure 4e, some of the coating may have spalled. However, the surface under the spalled region appears remarkably smooth suggesting that the coating may still have been protective of the surface. This may be even more remarkable given that the possible spalling appears to have developed between 40-85 minutes but the experiment lasted out to 205 minutes of intense exposure after which the profiles were collected. It is also possible that spalling is an edge effect present on small samples that would not be present on larger systems. The experiment was performed on a single set of samples for which assessment of measurement uncertainty was not within scope. Future work may reduce the time/intensity to make a more refined comparison and evaluate performance in the absence of edges. In net, however, the treated samples appeared to show diminished cavitation as evidenced by the minimal surface roughness with respect to the untreated sample.

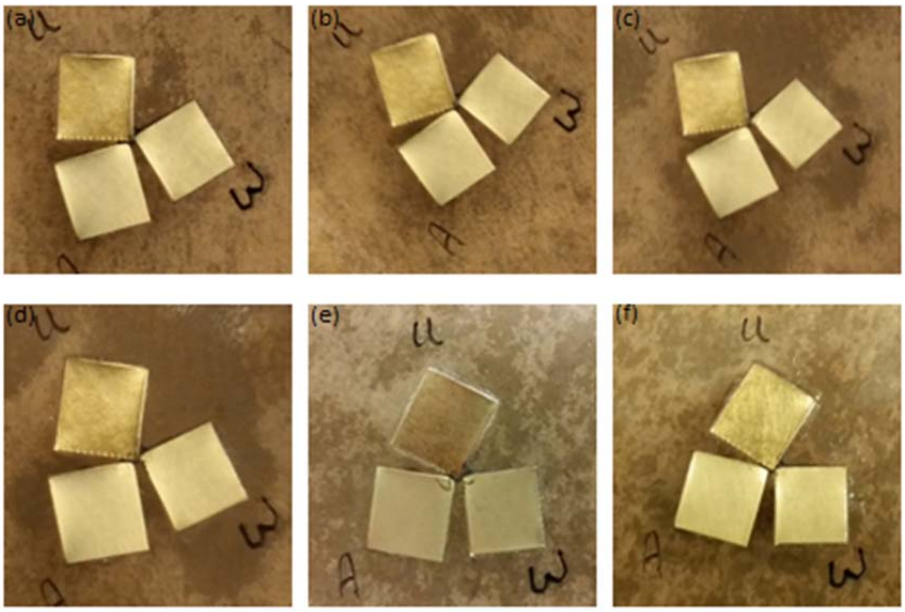

Figure 4. Images of the samples (a) 0 min (before testing started), (b) 10 min, (c) 40 min, (d) 85 min, (e) 145 min, and (f) 205 min after testing started. No further testing continued after panel f. The tip radius is approximately 3 mm.

[6] http://ir.veeco.com/news-events/press-releases/press-release-details/2009/Veeco-Ships-500th-Dektak-150-Surface-Profiler/default.aspx, downloaded 9-29-2016.

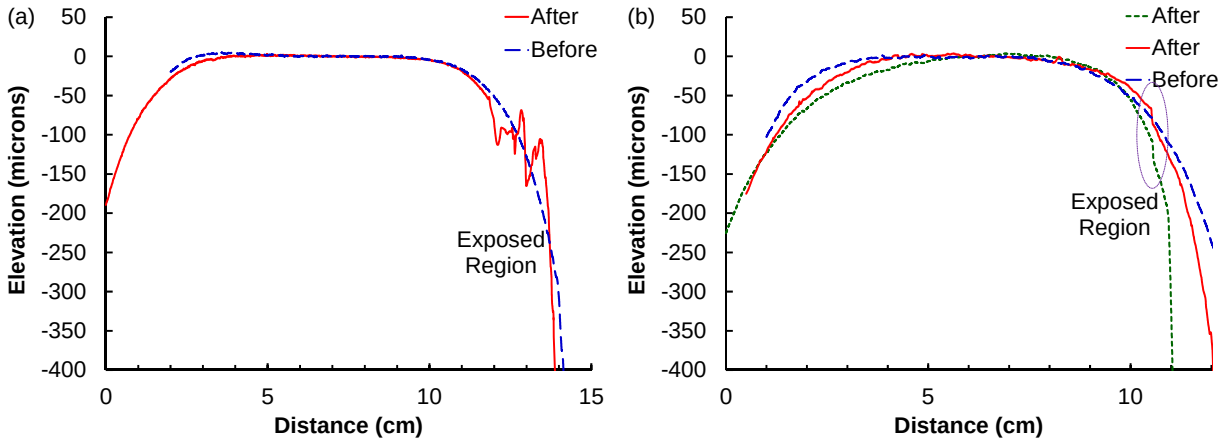

Figure 5. Profile scans before and after exposure of (a) the uncoated sample U and (b) the coated sample A. Post-processing of the data involved adjusting the slope and lateral offset to align the profiles on the left. Before and after scans do not line up precisely due to mismatch in sample alignment within the surface profilometer. Repeat scans in the same location were not performed within the scope of the project to confirm these observations.

Finally, several mechanisms (not evaluated further herein) may be responsible for cavitation reduction. Testing performed by GBS suggests that cavitation damage occurred on regions of a propeller that was not coated with their coating but did not occur where their coating was present. Mechanisms that may be responsible for this observation include:

- First, the coating may reduce heterogeneous nucleation of bubbles. Although most models of bubble growth and collapse are phrased as homogeneous nucleation of bubbles in the bulk, heterogeneously nucleated bubbles are perhaps most damaging because they are present right at the surface.[7] Because the surface is wetting as opposed to nonwetting, this will decrease bubble attachment.
- Second, the coating may repulse the bubbles away from the surface. It is possible that bubbles near the surface may form ionized plasmas during bubble collapse. This plasma may be polarized and then be either attracted or repulsed with respect to the charged surface. Given that the induced dipole would arise because of attraction of opposite charges and repulsion of like charges with respect to the surface charge, it is more likely than not an attractive force. However, the length scale over which these forces act is likely small in seawater given the small Debye and Bjeerum length scales on the order of a few nanometers or less.
- Third, the coating may prevent damage in analogy to a shock absorber. Van Terwisga, et al., describe the energy spectrum and its relationship to cavitation erosion, indicating that the threshold for damage is material-specific.[8] Damage may occur due to
    - Localized heating.[9] The temperature becomes very high during bubble collapse in a tightly localized area. It may be that silica surfaces require a much higher temperature to ionize than typical surfaces, in part explaining their resistance.

[7] http://ocw.tudelft.nl/courses/marine-technology/cavitation-on-ship-propellers/4-physics-of-cavitation-cavitation-inception/; http://web.mit.edu/hml/ncfmf/16CAV.pdf, downloaded 1/20/2016.
[8] http://deepblue.lib.umich.edu/handle/2027.42/5339, downloaded 1/20/2016.; http://deepblue.lib.umich.edu/bitstream/handle/2027.42/84241/CAV2?sequence=1, downloaded 1/20/2016.

    - Pressure waves. When a pressure wave from the collapsing bubble passes, it may be that a higher elastic modulus of the coating may minimize deformation of the coating layer in comparison to typical surfaces.
    - Reentrant jets.[10] These jets form near the center of the collapsing bubbles and are at high velocity for a very short time. It may be that the coating is more resistant to these jets than typical surfaces.[11]
    - Free radical formations. Silica enriched surfaces may be more resistant to free radical degradation than typical surfaces.
- Fourth, the coating may experience damage but be self-healing. Some ceramics are known to be self-healing,[12] though it has not been determined whether this coating's constituents are self-healing.

Summary

Based on these results and options, the following follow-on work may be informative.

1. Additional work to quantify the surface charge and slip in aqueous environments correlated with drag force measurements remains of interest. This may be performed in internal flow configurations such as in closed loop piping systems because the physics of flow is the same regardless of whether the flow is external to the material of interest or internal.
2. The influence of the coating on dynamic contact angles with and without electrical fields remains of interest in the context of drag reduction.
3. Additional experiments to evaluate the cavitation mechanism remains of interest. Several mechanisms have been listed above and additional experiments are needed to evaluate these quantitatively.

In summary, this may be a compelling candidate for the DOE Voucher Program or follow-on work in FY17.

Disclaimer

Battelle does not endorse products or services or recommend investments, nor does it undertake technology investigations for advertising, sales promotion, or endorsement.

Acknowledgements

This report was prepared with funding from the TAP program. A portion of the research was performed using EMSL, a DOE Office of Science User Facility sponsored by the Office of Biological and Environmental Research. We express appreciation to Jia Liu, Nathan Phillips, Christopher Clayton, and Hardeep Mehta who performed the experiments and assisted in their analysis. We also express appreciation to Kayte Denslow, A. Scott Lea, Mark Engelhard, Ronald Thomas, and Ashley Gilbert for expert guidance and administrative support. Finally, we express appreciation to Gary Spanner for project management and leadership.

[9] http://ocw.tudelft.nl/courses/marine-technology/cavitation-on-ship-propellers/4-physics-of-cavitation-cavitation-inception/, downloaded 1/20/2016.
[10] http://web.mit.edu/hml/ncfmf/16CAV.pdf, downloaded 1/20/2016.
[11] http://deepblue.lib.umich.edu/bitstream/handle/2027.42/84241/CAV2?sequence=1, downloaded 1/20/2016.
[12] http://link.springer.com/chapter/10.1007%2F978-3-642-35197-6_52#page-1, downloaded 1/20/2016.

Appendix: Notes on Electrohydrodynamic Modification to Drag

Given client interest in the possibility of electrohydrodynamic effects and the lack of similar derivations readily available in the open literature, the following brief derivation is appended to evaluate the influence of a surface charge on the drag force. The frictional component (as opposed to the form component) of drag may be estimated in the absence of slip by

$$F_{De} = \int_s \boldsymbol{n} \cdot \boldsymbol{\tau} \cdot \boldsymbol{t} dS,$$

where $\boldsymbol{t}$ and $\boldsymbol{n}$ is the tangential and normal vectors, $\boldsymbol{\tau}$ is the stress tensor, and S is the surface area. Bold denotes vectors or second order tensors. The stress tensor may be identified with both fluid stresses and Maxwell stresses. Only the latter are of interest in this analysis. The Maxwell stress tensor may be written as

$$\boldsymbol{\tau}^M = \varepsilon\varepsilon_o \left(\boldsymbol{EE} - \frac{1}{2}\boldsymbol{\delta E} \cdot \boldsymbol{E} \right),$$

where $\boldsymbol{E}$ is the electric field, ε is the dielectric constant, ε_o is the permittivity of free space, and $\boldsymbol{\delta}$ is the Kronecker delta. Substituting the second into the first leaves to first order

$$F_{De} = \varepsilon\varepsilon_o E_n E_t S,$$

where E_n and E_t are the normal and tangential components of the electric field. Assuming field separability, the linearized Poisson-Boltzmann equation gives the normal component of the electrostatic potential derives from

$$\phi = \frac{\kappa q}{\varepsilon\varepsilon_o} Exp\left[-\frac{x_n}{\kappa} \right],$$

where x_n is the length in the normal direction from the surface, q is the surface charge in charges per area, and κ is the well-known Debye-Huckle length. The negative gradient of this potential is the electric field from which

$$F_{De} = qE_t S$$

upon evaluation at x_n=0. The sign of the drag force depends on the signs of the surface charge and tangential component of the electric field. Surface charges in dry environments range over seven orders of magnitude from 0.12 mC/m^2 to as high as 10^3 C/m^2,[13] suggesting that drag force reduction may be significant.

[13] http://dx.doi.org/10.1063/1.2364497, downloaded 1/20/2016.